Quantum information processing by NMR using strongly coupled spins*

T. S. Mahesh[†,], Neeraj Sinha[†,#], Arindam Ghosh[†], Ranabir Das[†], N. Suryaprakash[‡], Malcolm H. Levitt[§], K. V. Ramanathan[‡] and Anil Kumar[†,‡,¶]**

[†]Department of Physics and [‡]Sophisticated Instruments Facility, Indian Institute of Science, Bangalore 560 012, India
[§]Department of Chemistry, University of Southampton, Southampton SO17 1BJ, England
**Present address: Francis Bitter Magnet Lab, Massachusetts Institute of Technology, Cambridge, Massachusetts 02139, USA
[#]Present address: Department of Chemistry, Iowa State University, Iowa 50011-3111, USA

The enormous theoretical potential of quantum information processing (QIP) is driving the pursuit for its practical realization by various physical techniques. Currently, nuclear magnetic resonance (NMR) has been the forerunner by demonstrating a majority of quantum algorithms. In NMR, spin-systems consisting of coupled nuclear spins are utilized as qubits. In order to carry out QIP, a spin-system has to meet two major requirements: (i) qubit addressability and (ii) mutual coupling among the qubits. It has been demonstrated that the magnitude of the mutual coupling among qubits can be increased by orienting the spin-systems in a liquid crystal matrix and utilizing the residual dipolar couplings. While utilizing residual dipolar couplings may be useful to increase the number of qubits, nuclei of the same species (homonuclei) might become strongly coupled. In strongly coupled spin-systems, spins lose their individual identity of being qubits. We propose that even such strongly coupled spin-systems can be used for QIP and the qubit-manipulation can be achieved by transition-selective pulses. We demonstrate experimental preparation of pseudopure states, creation of maximally entangled states, implementation of logic gates and implementation of Deutsch–Jozsa (DJ) algorithm in strongly coupled 2, 3 and 4 spin-systems. The energy levels of the strongly coupled 3 and 4 spin-systems were obtained using a Z-COSY experiment.

THE theoretical success of exploiting the quantum nature of physical systems in certain information processing tasks like prime factorization[1] and unsorted database search[2] has motivated the pursuit for the practical realization of quantum information processing (QIP)[3–5]. With the demonstration of many quantum algorithms, nuclear magnetic resonance (NMR) is now considered as a suitable test-bed for QIP. One of the main challenges for the progress of NMR–QIP is 'how to increase the number of qubits?' In this direction several attempts are being made, such as (i) find molecules with different chemical shifts and *J*-couplings, and (ii) use of dipolar and quadrupolar couplings. This article concentrates on one aspect: 'how to use dipolar couplings among homonuclear spins'. This problem is outlined in the following paragraphs.

In NMR, systems consisting of coupled spin-1/2 nuclei form qubits. In order to carry out QIP, the spin-system has to meet two main requirements: qubit addressability and mutual coupling among the qubits. In liquid-state NMR using isotropic fluids, the qubit addressability is normally provided by the differences in Larmor frequencies of the various spin-1/2 nuclei, while the mutual coupling is normally provided by the scalar (*J*) coupling among the nuclei connected by covalent bonds. The Hamiltonian for a *J*-coupled spin-system is[6],

$$\mathcal{H} = \mathcal{H}_Z + \mathcal{H}_J = \sum_i \omega_i I_{iz} + \sum_{i,\, j(i<j)} 2\pi J_{ij} (I_{iz} I_{jz} + I_{ix} I_{jx} + I_{iy} I_{jy}), \quad (1)$$

where $\mathcal{H}_Z$ is the Zeeman Hamiltonian, and $\mathcal{H}_J$ is the coupling Hamiltonian. When $2\pi J_{ij} \ll |\omega_i - \omega_j|$, the system is said to be weakly coupled, and the Hamiltonian can be approximated to[6],

$$\mathcal{H} = \sum_i \omega_i I_{iz} + \sum_{i,\, j(i<j)} 2\pi J_{ij} I_{iz} I_{jz}. \quad (2)$$

For qubit addressability, all ω_i should be sufficiently dispersed and all J_{ij} should be non-negligible (> 1 Hz) and unequal in magnitude. In such a circumstance, each spin can be treated as a qubit and the coupled nuclei as several qubits. The values of J_{ij} depend on the covalent bonds connecting spins *i* and *j*. They normally have a small range (< 10^2 Hz) and become too small (< 1 Hz) if the spins are connected by more than 4–5 covalent bonds. This places a natural limit on the number of qubits reachable by liquid-state NMR using *J*-couplings alone. To overcome this limitation, the possibility of using dipolar couplings was considered. The truncated Hamiltonian for dipolar interaction is[6,7],

*Dedicated to Prof. S. Ramaseshan on his 80th birthday.

¶For correspondence. (e-mail: anilnmr@physics.iisc.ernet.in)

$$\mathcal{H}_{\mathrm{D}} = \sum_{i,j(i<j)} 2\pi D_{ij}(3I_{iz}I_{jz} - \mathbf{I_i}\cdot\mathbf{I_j}). \quad (3)$$

The dipolar coupling D_{ij} between spins of gyromagnetic ratios γ_i and γ_j, whose inter-distance vector r_{ij} makes an angle θ_{ij} with the Zeeman magnetic field is of the form[6,7],

$$D_{ij} = \frac{\gamma_i\gamma_j\hbar}{4\pi r_{ij}^3}(1-3\cos^2\theta_{ij}). \quad (4)$$

Dipolar couplings among common nuclear species have larger magnitudes (~10^3 Hz) and longer range than scalar couplings. However, in isotropic liquids the time average of D_{ij} vanishes, while in solids there are too many dipolar couplings resulting in broad, unresolved lines and loss of qubit addressability. In molecules oriented in a liquid crystal matrix, while the intermolecular dipolar couplings are vanishingly small, the intramolecular dipolar couplings survive, scaled down by the order parameter S_{ij} of the liquid crystal[7,8],

$$D_{ij}^{\mathrm{ori}} = \frac{\gamma_i\gamma_j\hbar}{4\pi r_{ij}^3}\langle 1-3\cos^2\theta_{ij}\rangle = -\frac{\gamma_i\gamma_j\hbar}{4\pi r_{ij}^3}S_{ij}. \quad (5)$$

In such systems one obtains a finite number of sharp, well-resolved spectral lines making it possible to use such systems for NMR–QIP[9–13]. In the NMR–QIP experiments implemented so far, the systems have been chosen such that either (i) $2\pi(J_{ij} + 2D_{ij}) \ll |(\omega_i - \omega_j)|$, yielding weakly coupled spin-systems, which is the case for the heteronuclear spin-systems[9,10] or (ii) the coupling $2(J_{ij} + 2D_{ij})$ is finite and $|\omega_i - \omega_j| = 0$, i.e. equivalent-spins case[11,12]. In the latter case, the symmetry filtering of energy levels becomes increasingly difficult for higher number of qubits[11–13]. Even though the heteronuclear spins oriented in liquid crystal matrix are excellent for QIP since they provide good qubit addressability as well as large mutual coupling, the use of more than 3–4 heteronuclear spins is limited by the extensive hardware requirements. Therefore, for reaching larger number of qubits, one needs to utilize homonuclear (nuclei of same species having same γ, but different chemical shifts) spins oriented in a liquid crystal.

Homonuclear spins oriented in a liquid crystal generally become strongly coupled, since the dipolar couplings become comparable to or more than the differences in Larmor frequencies $|\omega_i - \omega_j|$. In such a situation, the Zeeman and the coupling parts of the Hamiltonian do not commute. Therefore, the eigenstates of strongly coupled spins are obtained as the linear combinations of product states of various spins, and the individual spins can no more be treated as qubits. We propose and demonstrate here that the 2^N eigenstates of a coupled N-spin 1/2 system can be treated as an N qubit system, even in the presence of strong coupling. A similar idea has already been used in demonstration of QIP using quadrupolar ($S > 1/2$) nuclei oriented in high magnetic field, where the $2S + 1$ non-equidistant energy levels have been treated as N-qubit systems, where $2^N = 2S + 1$. So far $S = 3/2$ and 7/2 have been utilized, respectively as 2 and 3 qubit systems[14–18] for various NMR–QIP.

While substantial work has been carried out in NMR–QIP using weakly coupled spin-systems[19], till now the use of the strongly coupled spin-systems for QIP has not been experimentally demonstrated, presumably because (i) spin-selective pulses are not defined in the case of strongly coupled spins[6], and (ii) there is difficulty in constructing a general unitary operator using the evolution under scalar coupling[20]. The problem of using scalar coupling evolution of a strongly coupled two-spin-system for a general unitary transform has recently been addressed theoretically, but extending to an N-spin-system is complicated[21]. However, we note that unlike spin-selective pulses, the transition-selective pulses are well-defined even in strongly coupled spin-systems[6], and hence it is possible to construct a unitary transformation using transition-selective pulses. In the next section we demonstrate NMR–QIP on a strongly coupled two-spin-system in isotropic medium by preparing pseudopure states, implementing Deutsch–Jozsa (DJ) algorithm, creating Einstein–Podolsky–Rosen (EPR) state and implementing logic gates. Next, we describe the creation of Greenberger–Horne–Zeilinger (GHZ) states and implementation of two-qubit DJ algorithm on a strongly coupled three-spin-system in an oriented medium after labelling the transitions using the Z-COSY experiment. Labelling of transitions, preparation of pseudopure states, and implementation of gates on a strongly coupled four-spin system are then demonstrated.

In this study the strongly coupled systems used are given in Table 1.

The experiments have been carried out on a Bruker DRX-500 NMR spectrometer at 300 K.

Strongly coupled two-spin system

The four eigenstates of a strongly coupled two-spin-system (of spin 1/2 nuclei; AB spin-system) in isotropic medium are $|\alpha\alpha\rangle$, $\cos\Theta|\alpha\beta\rangle + \sin\Theta|\beta\alpha\rangle$, $\cos\Theta|\beta\alpha\rangle - \sin\Theta|\alpha\beta\rangle$ and $|\beta\beta\rangle$ (Figure 1 *a*), where $\Theta = \frac{1}{2}\tan^{-1}(2\pi J_{AB}/(\omega_A - \omega_B))$[6]. These eigenstates are labelled respectively as $|00\rangle$, $|01\rangle$, $|10\rangle$ and $|11\rangle$, thus forming a two-qubit system (Figure 1 *b*). To demonstrate QIP on such a system, we have taken the strongly coupled ^{1}H spins of trisodium citrate (Figure 1 *c*). In this system, the scalar coupling (J) is 15 Hz, the difference in Larmor frequencies (Δf) is 55.5 Hz, and the strong coupling parameter (Θ) is 7.6°. The equilibrium spectrum of the system is shown in Figure 1 *d*.

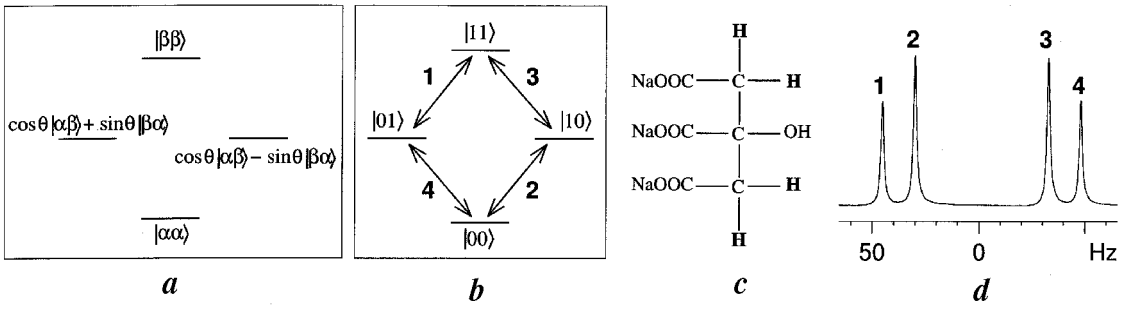

Figure 1. ***a***, Eigenstates of a strongly coupled two-spin-system; ***b***, Qubit labelling; ***c***, Trisodium citrate yielding a strongly coupled two-spin-system, and ***d***, Equilibrium 500 MHz ^{1}H spectrum of ***c***.

Table 1. The various samples used for QIP

Sample	Solvent	Isotropic/ oriented	No. of qubits
Trisodium citrate	D_2O	Isotropic	2
Organometallic compound (I)	$CDCl_3$	Isotropic	2
1-Bromo-2,3-dichlorobenzene	ZLI-1132	Oriented	3
2-Chloroiodobenzene	ZLI-1132	Oriented	4

Preparation of pseudopure states

In QIP, the computation normally begins from a definite initial state known as a pure state[3,4]. In NMR, however, because of the small energy gaps, it is not possible to realize a pure state wherein the whole population is in one energy level, since it requires very low temperatures as well as very high magnetic fields. However, an alternate solution was discovered to overcome this problem[22,23]. In thermal equilibrium, NMR density matrix can be written as

$$\rho = 2^{-N}\{I + \varepsilon\rho_{\text{dev}}\}. \tag{6}$$

The first part is a normalized unit matrix which corresponds to a uniform population background. The second part containing the traceless deviation density matrix ρ_{dev} (with a small coefficient $\varepsilon \sim 10^{-5}$) evolves under various NMR Hamiltonians, and gives measurable signal. It was observed independently by Cory *et al.*[22] and Chuang *et al.*[23], that by applying a certain pulse sequence to the system in equilibrium, we can prepare the so-called pseudopure density matrix,

$$\rho_{\text{pps}} = 2^{-N}\{(1-\varepsilon'/2^N)I + \varepsilon'\rho_{\text{pure}}\}. \tag{7}$$

The first part is again a scaled unit matrix, but the second part corresponds to a pure state. Such pseudopure states mimic pure states[22,23]. Many methods have been proposed for the preparation of pseudopure states, including spatial averaging[22,24], temporal averaging[25], logical labelling[23,26,27], and spatially averaged logical labelling[28]. Some of the other methods include the preparation of pseudopure states via cat states[29] and preparation of pair of pseudopure states[11]. Both *J*-evolution and transition-selective pulse methods have been utilized for preparation of pseudopure states[13,16,22,25,27,30].

We have adopted the method of spatial averaging using transition-selective pulses. The Boltzmann distribution of populations in high-temperature high-field approximation is linear with energy gap. The equilibrium deviation populations (in excess of a large uniform background population) of a homonuclear two-spin-system are schematically given in Figure 2 *a*. For creating a pseudopure state all the populations except one of the states have to be equalized. This distribution can be achieved by a sequence of transition-selective pulses intermittent with field-gradient pulses to destroy any coherence created in the process.

A transition-selective pulse of nutation angle θ and of any transverse phase between states (i, j), changes the populations as follows:

$$p_i' = p_i \cos^2(\theta/2) + p_j \sin^2(\theta/2),$$

$$p_j' = p_j \cos^2(\theta/2) + p_i \sin^2(\theta/2). \tag{8}$$

To prepare the $|00\rangle$ pseudopure state (Figure 2 *b*) from equilibrium (Figure 2 *a*), we use a sequence $[(\theta)^{|10\rangle\leftrightarrow|11\rangle} - G_z - (90°)^{|01\rangle\leftrightarrow|11\rangle} - G'_z]$ (pulses are applied from left to right), and it is inferred from the deviation populations of Figure 2 *a* and *b*, that θ should be such that $\cos^2(\theta/2) = 2/3$. This yields $\theta = 70.5°$. On the other hand, $\theta = 90°$ equalizes the populations of the two levels to an average value. Thus, the $|00\rangle$ pseudopure state is prepared by the pulse sequence $[(70.5°)^{|10\rangle\leftrightarrow|11\rangle} - G_z - (90°)^{|01\rangle\leftrightarrow|11\rangle} - G'_z]$ and the corresponding spectrum is given in Figure 2 *b*. The $|01\rangle$ and $|10\rangle$ pseudopure states (Figure 2 *c* and *d*) are prepared by applying $(180°)^{|00\rangle\leftrightarrow|01\rangle}$ and $(180°)^{|00\rangle\leftrightarrow|10\rangle}$ pulses, respectively after creating the $|00\rangle$ pseudopure state. The $|11\rangle$ pseudopure state (Figure 2 *e*) is prepared by the pulse sequence $(70.5°)^{|00\rangle\leftrightarrow|01\rangle} - G_z - (90°)^{|00\rangle\leftrightarrow|10\rangle} - G'_z$. The observed intensities in the spectra on the left-hand-side of Figure 2 correspond to the created population distribution and hence confirm the creation of the pseudopure states.

DJ algorithm

The DJ algorithm is one of the first quantum algorithms which successfully demonstrated the power of QIP[31,32]. The task of the DJ algorithm is to distinguish between two classes of many-input-one-output functions, constant and balanced. Constant functions are those functions in which all the outputs are same independent of inputs; and balanced functions are those in which half the number of inputs gives one output and the other half gives another output. Classically, given a function of n input bits, it takes $2^{n-1} + 1$ function-calls on an average, to determine whether the function is constant or balanced, whereas DJ algorithm needs only one function-call for any number of qubits. The DJ algorithm has been implemented in NMR using scalar-coupling evolution as well as spin and transition-selective pulses[27,33–36]. We have followed Cleve's version of the DJ algorithm which requires one extra work qubit[32]. The circuit diagram and the NMR pulse sequence for implementing 1-qubit DJ algorithm are shown in Figure 3 *a* and *b*, respectively. The experiment begins with the $|00\rangle$ pseudopure state. An initial $(\pi/2)_{-y}$ pulse (the pseudopure Hadamard operation[34]) on all the qubits creates a superposition. It may be noted that unlike weakly-coupled spins, the superposition created here is not uniform in the eigenbasis, since the coefficients of various eigenstates are different. However, as is shown here, it is still possible to distinguish between the different classes of functions. The Hadamard operation is followed by an unitary operator U_f corresponding to the given function f. The unitary operator carries out the transformation $|r, s\rangle \xrightarrow{U_f} |f(s) \oplus r, s\rangle$, where $|r\rangle$ and $|s\rangle$ are the states of the work-qubit and the input-qubit, respectively. The four different one-qubit functions and the corresponding unitary operators as well as r.f. pulses are listed in Table 2. The test for a balanced function is that the transitions of input-qubit will gain opposite phases at the end of the algorithm. The experimental results corresponding to all the four functions f_1, f_2, f_3 and f_4 along with their corresponding simulated spectra are given in Figure 3 *c–f*. From the spectra we can identify that functions f_1 and f_2 are constant, since the transitions 1 and 2 are of same phase, whereas f_3 and f_4 are balanced, since the transitions 1 and 2 are of opposite phase (transition numbers are from Figure 2 *a*).

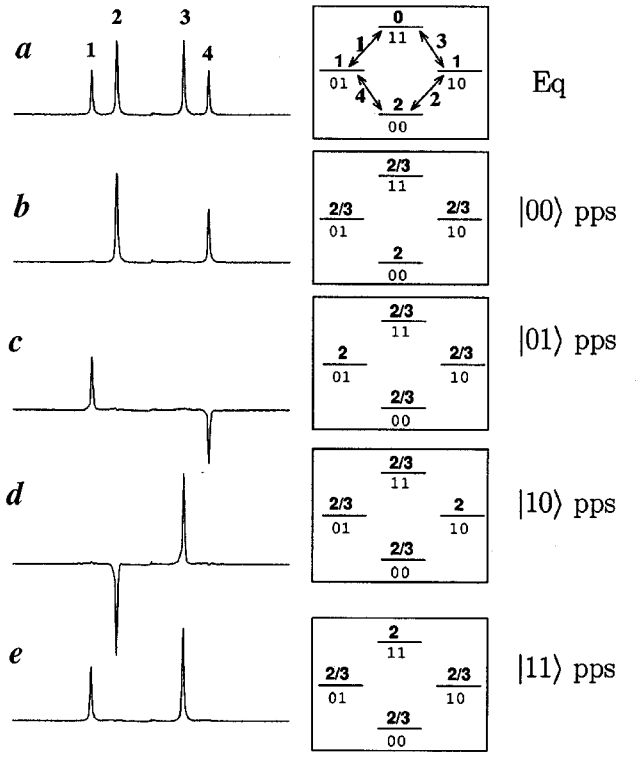

Figure 2. ***a***, Equilibrium spectrum of trisodium citrate, and spectra corresponding to various pseudopure states: ***b***, $|00\rangle$; ***c***, $|01\rangle$; ***d***, $|10\rangle$, and ***e***, $|11\rangle$. Numbers above the energy levels indicate populations and binary numbers below the levels indicate labels. Transitions are also indentified as 1, 2, 3 and 4 in (***a***). Pulse sequences applied to prepare each pseudopure state are explained in the text. Transition-selective pulses used were of length 100 ms and gradient pulse was of length 1 ms and strength 10 G/cm. Each spectrum was obtained by a non-selective high-power pulse of duration 1 μs, corresponding to a flip-angle of 10°.

Creation of an EPR state

EPR pairs are the maximally entangled pairs of the form

$$\frac{1}{\sqrt{2}}(|00\rangle \pm |11\rangle) \text{ or } \frac{1}{\sqrt{2}}(|01\rangle \pm |10\rangle), \quad (9)$$

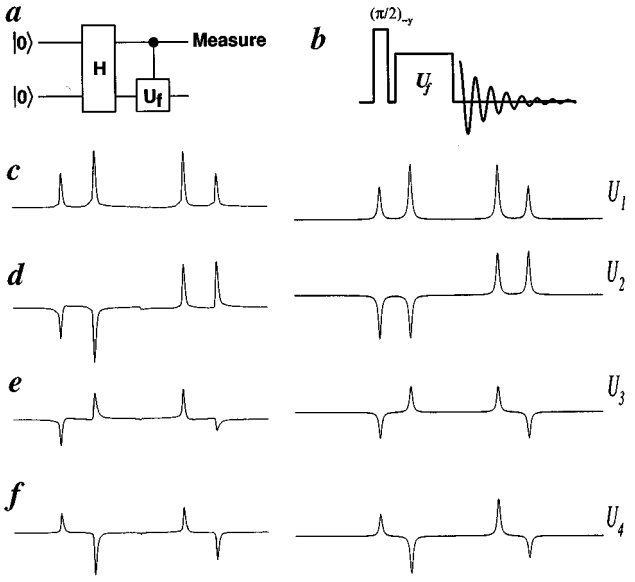

Figure 3. Implementation of DJ algorithm. ***a***, Quantum circuit. ***b***, Experimental scheme for the implementation of DJ algorithm. ***c***, ***d***, Experimental spectra corresponding to the two constant functions of U_1 and U_2 respectively. ***e***, ***f***, Spectra corresponding to the two balanced functions of U_3 and U_4 respectively. Expected spectra for all the four functions are given on the right-hand-side.

Table 2. Functions, unitary operators and r.f. pulses for one-qubit DJ algorithm

	Constant		Balanced	
	f_1	f_2	f_3	f_4
0	0	1	0	1
1	0	1	1	0
U_f	$\begin{pmatrix}1&0&0&0\\0&1&0&0\\0&0&1&0\\0&0&0&1\end{pmatrix}$	$\begin{pmatrix}0&1&0&0\\1&0&0&0\\0&0&0&1\\0&0&1&0\end{pmatrix}$	$\begin{pmatrix}1&0&0&0\\0&1&0&0\\0&0&0&1\\0&0&1&0\end{pmatrix}$	$\begin{pmatrix}0&1&0&0\\1&0&0&0\\0&0&1&0\\0&0&0&1\end{pmatrix}$
Pulse	No pulse	$(\pi)^{\|00\rangle \leftrightarrow \|01\rangle} - (\pi)^{\|10\rangle \leftrightarrow \|11\rangle}$	$(\pi)^{\|10\rangle \leftrightarrow \|11\rangle}$	$(\pi)^{\|00\rangle \leftrightarrow \|01\rangle}$

Table 3. Transition numbers of eq. (10) and corresponding phases of r.f. pulses for creating $|00\rangle + |11\rangle$ EPR state. Transition numbers are from Figure 1 *b*

Expt. no.	k	l	ϕ_1	ϕ_2	Expt. no.	k	l	ϕ_1	ϕ_2
1	2	3	x	$-x$	5	4	1	x	$-x$
2	2	3	$-x$	x	6	4	1	$-x$	x
3	2	3	y	y	7	4	1	y	y
4	2	3	$-y$	$-y$	8	4	1	$-y$	$-y$

which are not reducible into product states of individual qubits[3]. The non-local correlation exhibited by these pairs has no classical equivalence, and is exploited in many branches of QIP, including quantum computation and quantum teleportation[3,4]. EPR states of a pair of weakly-coupled nuclear spins have been earlier created by NMR using spin-selective pulses and evolution of coupling[9].

Here, we demonstrate the creation of EPR state on the above strongly coupled two-spin-system using transition-selective pulses and tomograph the result using non-selective pulses. Starting from $|00\rangle$ pseudopure state, the EPR state $(|00\rangle + |11\rangle)/\sqrt{2}$ can be created by applying the pulse sequence (pulses are to be applied from left to right)

$$\left[\left(\frac{\pi}{2}\right)_{\phi_1}^{k} \cdot (\pi)_{\phi_2}^{l}\right], \tag{10}$$

where k and l are the transitions, and ϕ_1 and ϕ_2 are the phases as shown in Table 3. For example, the unitary operator U for the pulse sequence

$$\left[\left(\frac{\pi}{2}\right)_{x}^{2} \cdot (\pi)_{-x}^{3}\right]$$

is

$$U = \exp(i\pi I_x^{|10\rangle\leftrightarrow|11\rangle}) \cdot \exp(-i\tfrac{\pi}{2} I_x^{|00\rangle\leftrightarrow|10\rangle})$$

$$= \frac{1}{\sqrt{2}}\begin{pmatrix}1&0&-i&0\\0&\sqrt{2}&0&0\\0&0&0&i\sqrt{2}\\1&0&i&0\end{pmatrix}, \tag{11}$$

where the operators are however applied from right to left. EPR state is obtained by applying U on $|00\rangle$ pseudo-pure state

$$U \cdot \begin{pmatrix}1&0&0&0\\0&0&0&0\\0&0&0&0\\0&0&0&0\end{pmatrix} \cdot U^{\dagger} = \frac{1}{2}\begin{pmatrix}1&0&0&1\\0&0&0&0\\0&0&0&0\\1&0&0&1\end{pmatrix}. \tag{12}$$

A phase-cycle over different combinations given in Table 3 helps reduce errors in the off-diagonal elements. Figure 4 *a* shows the experimental equilibrium spectrum and Figure 4 *b* shows the experimental spectrum after creating the EPR state. Since the EPR state does not consist of any single quantum coherence, no signal is obtained (Figure 4 *b*). The corresponding simulated spectra are shown in Figure 4 *f* and *g*.

To verify the creation of the EPR state, it is necessary to tomograph the complete density matrix. Tomography in NMR is normally carried out using spin-selective pulses obtaining a series of one-dimensional NMR experiments, each giving a linear equation of different elements of the density matrix[26]. However, in the case of strongly coupled systems all operations, including tomography exclude the use of spin-selective pulses and demand either non-selective pulses or transition-selective pulses or both. Recently, a robust method for tomography was suggested based on two-dimensional Fourier spectroscopy, which utilizes only non-selective pulses[37]. This method involves:

(i) a one-dimensional experiment for measuring diagonal elements: $[G_z - 10_x^{\circ} - t]$, and
(ii) a two-dimensional multiple quantum experiment for measuring all off-diagonal elements:

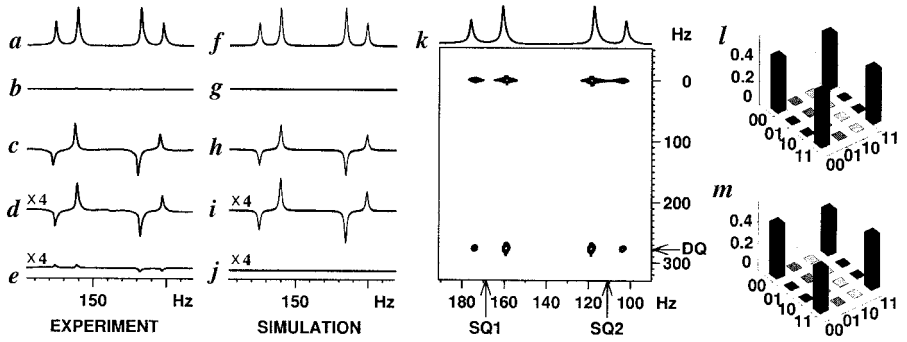

Figure 4. Creation and tomography of $(|00\rangle + |11\rangle)\sqrt{2}$ EPR state. Spectra in ***a***–***e*** are experimental and in ***f***–***j***, are simulated, corresponding to various steps of creation and tomography. ***a***, ***f***, Equilibrium spectra; ***b***, ***g***, Spectra after creation of EPR state (no single quantum signal observed); ***c***, ***h***, Spectra of diagonal part measured by the pulse sequence (EPR) – G_z – 10°_x ; ***d***, ***i***, Spectra obtained by the sequence (EPR) – $(\pi/4)_x$; ***e***, ***j***, Spectra obtained by (EPR) – $(\pi/4)_y$; ***k***, Two-dimensional spectrum to measure the off-diagonal elements. This spectrum clearly shows the double quantum coherence present in the EPR state. Axial peaks at zero frequency originate from the longitudinal relaxation of EPR state during t_1 period which is detected due to the imperfection of the 90° r.f. pulse following the t_1 period. The theoretical (***l***), and experimental (***m***) density matrices of EPR state. Spectra in ***d***, ***e***, are used for calculating the scaling between diagonal and off-diagonal measurements. While plotting, the spectra shown in ***d***, ***e***, ***i***, ***j*** are scaled-up by a factor of 4. Pseudopure state and EPR state are created using transition-selective pulses of length 100 ms. An eight-step cycle (shown in Table 3) was employed to minimize the errors.

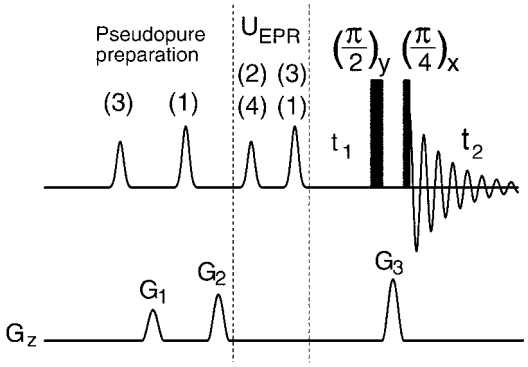

Figure 5. Pulse sequence for creation and tomography of EPR state. Numbers within parentheses indicate transition numbers as shown in Figure 1 ***d***. U_{EPR} is applied on transitions [(2), (3)] or [(4), (1)] as described in eq. (10) and Table 3. G_1, G_2 and G_3 are field-gradient pulses of different strengths along the $\hat{z}$-direction.

$$[t_1 - (\pi/2)_y - G_z - (\pi/4)_{-y} - t_2]. \quad (13)$$

The scheme involves only non-selective pulses and therefore, it is not only simple and accurate, but also applicable to strongly coupled systems. The result of measurement of diagonal elements of the EPR state [experiment (i)] is shown in Figure 4 *c* and the corresponding simulated spectrum is shown in Figure 4 *h*. Figure 5 shows the complete pulse-sequence for creation of EPR state followed by measurement of the off-diagonal elements [experiment (ii)]. The resulting 2D spectrum of the experiment is given in Figure 4 *k*, which clearly shows the double quantum peaks corresponding to the EPR state. No zero quantum or single quantum peaks are observed[37].

Since the diagonal and off-diagonal terms are measured by two different schemes, it is necessary also to determine the scaling between the two measurements. Normally, this is achieved by comparing single quantum terms in the two-dimensional experiment with the spectrum obtained by direct detection of the density matrix[37]. However, since no single quantum coherence is present in the EPR density matrix, we carried out two additional one-dimensional experiments: (iii) $[(\pi/4)_y - t]$ and (iv) $[(\pi/4)_x - t]$ after creation of the EPR pair. Experimental spectra corresponding to (iii) and (iv) are shown in Figure 4 *d* and *e*, respectively, and the corresponding simulated spectra are shown in Figure 4 *i* and *j*, respectively. The signals in Figure 4 *d* are proportional to the sum of the amplitudes of diagonal and double quantum coherences of the EPR state, while those in Figure 4 *e*, are proportional to the differences (when single quantum coherences are not present as in the present case). Since in a perfect EPR state the diagonal elements and double quantum coherences are equal, the spectrum of Figure 4 *e*, should have no signal, as is evident from the simulated spectrum of Figure 4 *j*. The signals of Figure 4 *e* compared to Figure 4 *d* are measures of experimental errors, which in the present case are estimated to be less than 15%. The complete density matrices corresponding to the theoretical and experimentally obtained EPR state are shown in Figure 4 *l* and *m*.

Implementation of logic gates

Logic gates have been implemented earlier by one- and two-dimensional NMR using weakly-coupled spin-1/2

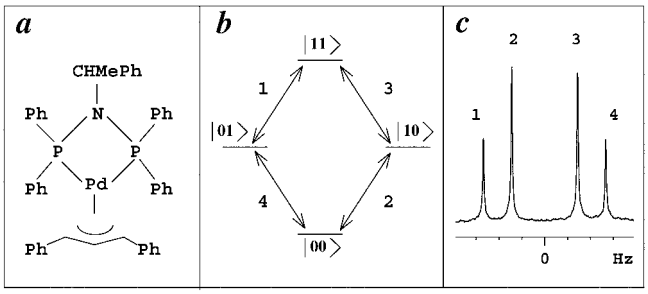

Figure 6. ***a***, Organometallic compound (I) in which the two phosphorus (^{31}P) nuclei constitute a two-spin-system. ***b***, Energy level diagram of the two-spin-system. ***c***, Equilibrium phosphorus spectrum recorded at 202 MHz in a magnetic field of 11.7 T.

nuclei as well as quadrupolar nuclei[13,16,24,38–41]. We demonstrate here the first implementation of a complete set of 24 one-to-one logic gates in a 2-qubit system using strongly coupled spin-1/2 nuclei. The system chosen for this purpose are the two phosphorus nuclei of the organometallic compound (I) shown in Figure 6 *a*. The energy level diagram and the equilibrium phosphorus spectrum of this molecule in isotropic liquid state are given in Figure 6 *b* and *c*, respectively. Starting from equilibrium, the logic gates were implemented using sequences of transition-selective pulses. The final populations were mapped by a small-angle (10°), non-selective pulse. The spectra corresponding to final populations of all the 24 logic gates are given in Figure 7. The unitary transforms and pulse sequences for implementation of these gates are given in ref. 39 with the modification that the r.f. power has been adjusted for a given angle of flip for the two inner versus the two outer transitions.

Strongly coupled three-spin system

The system and labelling of transitions

The system chosen are the three strongly coupled protons of 3-bromo-1,2-dichlorobenzene (Figure 8) oriented in the nematic liquid crystal ZLI-1132. The equilibrium spectrum of the system at 300 K obtained from DRX 500 MHz spectrometer is shown in Figure 8. There are only nine out of a total of 15 possible single quantum transitions with observable intensity in this spin-system. Construction of energy level diagram and labelling of transitions were performed using a Z-COSY experiment[42].

The Z-COSY spectrum along with cross-sections parallel to ω_2 axis at various transitions is given in Figure 9. The zero-quantum artifacts were suppressed in the Z-COSY experiment by incrementing a delay synchronized with t_1 increment[43]. The connectivity matrix is obtained by the MATLAB-assisted automation:

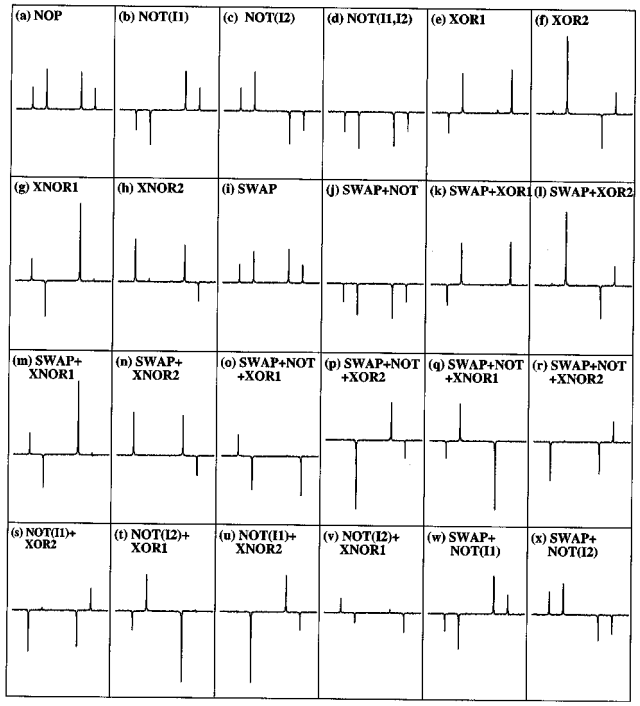

Figure 7. Implementation of 24 one-to-one logic gates. Starting from equilibrium all the gates were implemented using sequences of transition-selective pulses and non-selective pulses. The unitary transforms and pulse sequences for implementation of these gates are given in ref. 39. Gaussian-shaped pulses of 100 ms duration were used as selective pulses. The r.f. power has been calibrated for a given angle of flip for the two inner versus the two outer transitions. A sine-bell-shaped gradient was applied after implementation of each selective pulse, to kill any coherences created due to imperfection of pulses. Final populations were mapped by a small-angle (10°), non-selective pulse.

$$\begin{array}{c|cccccccc} & 1 & 2 & 3 & 4 & 5 & 6 & 7 & 8 \\ \hline 1 & 0 & 0 & -1 & 1 & 0 & 0 & 1 & 0 \\ 2 & 0 & 0 & 1 & -1 & -1 & 0 & 0 & 1 \\ 3 & -1 & 1 & 0 & 0 & 1 & 0 & 0 & 0 \\ 4 & 1 & -1 & 0 & 0 & 0 & 0 & -1 & 1 \\ 5 & 0 & -1 & 1 & 0 & 0 & 1 & -1 & 0 \\ 6 & 0 & 0 & 0 & 0 & 1 & 0 & 1 & -1 \\ 7 & 1 & 0 & 0 & -1 & -1 & 1 & 0 & 0 \\ 8 & 0 & 1 & 0 & 1 & 0 & -1 & 0 & 0 \end{array}. \quad (14)$$

The constructed energy level diagram for the above connectivity matrix is shown in Figure 10. The ninth transition shown by a dashed line belongs to the transition $011 \leftrightarrow 100$, and is not connected to any other observed transitions. Therefore, the transition did not show any connectivity to other transitions in the Z-COSY experiment (Figure 9) and is marked as * in Figure 8. It turns out that these nine transitions are sufficient to carry out certain QIP operations as shown in the following sections.

Preparation of pseudopure state

We have used the method of 'POPS' to prepare a pair of pseudopure states on this three-spin strongly coupled system[11]. POPS requires only two population distributions: (i) equilibrium populations (Figure 11 *a*) and (ii) equilibrium populations changed by a single transition-selective π pulse on a given transition (Figure 11 *b*). Subtraction of (ii) from (i) yields effectively, a pair of pseudopure states $|000\rangle\langle 000| - |001\rangle\langle 001|$ (Figure 11 *c*).

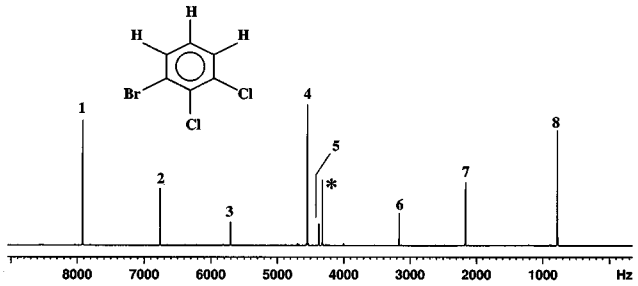

Figure 8. Equilibrium proton spectrum of 3-bromo-1,2-dichlorobenzene oriented in ZLI-1132 at 500 MHz. Transitions are labelled from left to right. The ninth transition marked ∗ did not show connectivity to other transitions (Figure 9), and belongs to the lone transition between 011 and 100 (marked by dashed line in Figure 10).

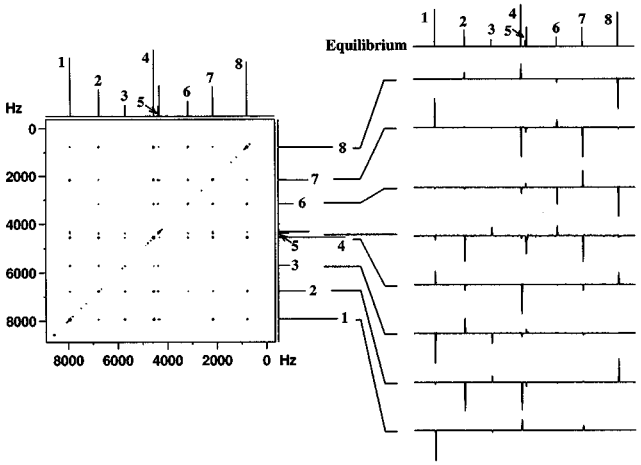

Figure 9. Z-COSY spectrum of oriented 3-bromo-1,2-dichlorobenzene. Equilibrium spectrum and cross-sections of the Z-COSY spectrum are shown on the right-hand-side.

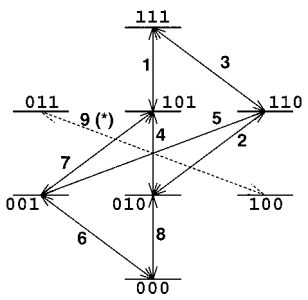

Figure 10. Energy level diagram of oriented 3-bromo-1,2-dichlorobenzene constructed using the Z-COSY spectrum shown in Figure 9. Transitions are labelled as in Figure 8. Only nine transitions are assigned. The remaining transitions have very low intensity.

Creation of $|GHZ\rangle\langle GHZ| - |001\rangle\langle 001|$ state

Entanglement between many particles is essential for most quantum communication schemes, including error-correction schemes and secret-key-distribution network[5]. GHZ states are three-spin entangled states of the form[44,45]

$$|\mathrm{GHZ}\rangle = \frac{1}{\sqrt{2}}(|000\rangle + |111\rangle). \quad (15)$$

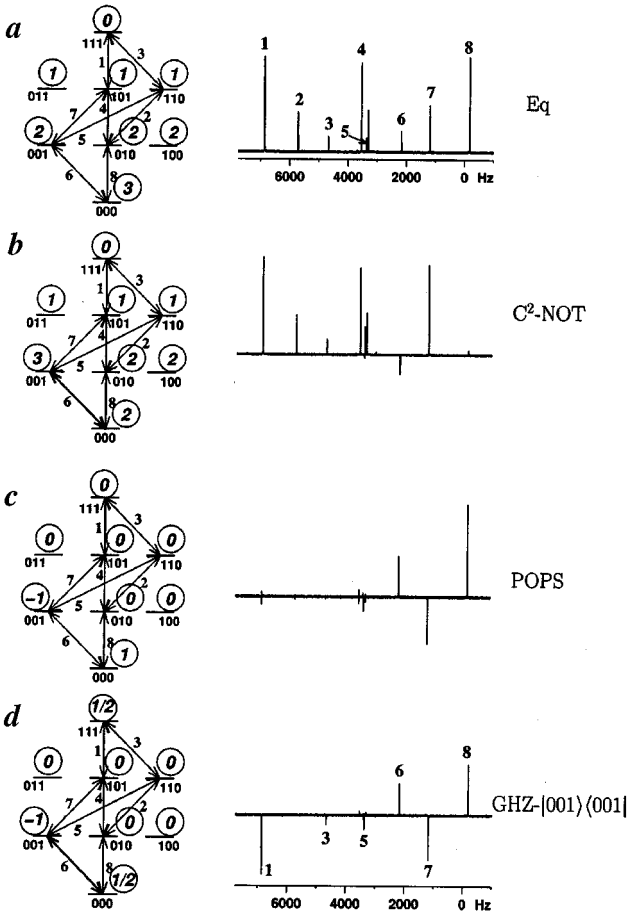

Figure 11. Preparation of GHZ state on the three-spin strongly coupled system of Figure 8. Energy levels, transitions and representative deviation populations (numbers inside circles) are shown on the left-hand-side and the corresponding spectra are shown on the right-hand-side. ***a***, Equilibrium deviation populations and the corresponding spectrum; ***b***, Deviation populations and spectrum obtained after inverting the transition 6, and ***c***, Deviation populations and spectrum obtained by subtracting ***b*** from ***a***. Deviation populations and the spectrum in ***c*** correspond to the pair of pseudopure states: $|000\rangle\langle 000| - |001\rangle\langle 001|$. ***d***, Population distribution and spectrum corresponding to the state $|GHZ\rangle\langle GHZ| - |001\rangle\langle 001|$. All spectra were recorded using a final small-angle (10°) detection pulse to maintain linear response, such that the intensities are proportional to the population differences of the two involved levels only.

Table 4. The 16-step phase-cycle for preparing GHZ state. The pulse-sequence is given in eq. (17)

	ϕ_1	ϕ_2	ϕ_3		ϕ_1	ϕ_2	ϕ_3		ϕ_1	ϕ_2	ϕ_3		ϕ_1	ϕ_2	ϕ_3
1	y	y	y	5	y	x	$-x$	9	x	y	$-x$	13	x	x	$-y$
2	y	$-y$	$-y$	6	y	$-x$	x	10	x	$-y$	x	14	x	$-x$	y
3	$-y$	y	$-y$	7	$-y$	x	x	11	$-x$	y	x	15	$-x$	x	y
4	$-y$	$-y$	y	8	$-y$	$-x$	$-x$	12	$-x$	$-y$	$-x$	16	$-x$	$-x$	$-y$

The three particles in GHZ state exhibit one of the strangest correlations that cannot be explained by any hidden variable theory[44,45]. A set of measurements carried out on the three particles in GHZ state prepare the particles in a classically impossible correlated state[5]. In NMR, the GHZ state was first created by Laflamme *et al.*[46]. The correlations of the GHZ state have been studied using NMR by Nelson *et al.*[47].

Preparation of the GHZ state requires preparing a pseudopure initial state, like $|000\rangle$. However, since we have prepared a pair of pseudopure states as the initial state, we will be actually preparing a state

$$|\mathrm{GHZ}\rangle\langle\mathrm{GHZ}| - |001\rangle\langle 001|. \tag{16}$$

This state differs from the GHZ state only in the diagonal elements and therefore retains the essential correlations of the GHZ state.

The GHZ state can be created from the $|000\rangle$ pseudopure state using a cascade of three transition-selective pulses (i) $(\pi/2)_{\phi_1}$ pulse on the transition 8, (ii) $(\pi)_{\phi_2}$ pulse on the transition 4 and (iii) $(\pi)_{\phi_3}$ pulse on the transition 1. The pulse sequence is,

$$\left[\left(\frac{\pi}{2}\right)^{(8)}_{\phi_1} \cdot \pi^{(4)}_{\phi_2} \cdot \pi^{(1)}_{\phi_3}\right], \tag{17}$$

where pulses are to be applied from left to right. The phases ϕ_1, ϕ_2 and ϕ_3 of the pulses can be any one of the 16 possible combinations, as shown in Table 4. A phase-cycle over these combinations helps reduce the errors in the off-diagonal elements.

The unitary operator for the above pulse-sequence can be written as,

$$U_{\mathrm{GHZ}} = \exp(-i\pi I^{(1)}_{\phi_3}) \cdot \exp(-i\pi I^{(4)}_{\phi_2}) \cdot \exp\left(-i\frac{\pi}{2} I^{(8)}_{\phi_1}\right), \tag{18}$$

where $I^{(1)}_{\phi_3}$, $I^{(4)}_{\phi_2}$ and $I^{(8)}_{\phi_1}$ are the single transition operators on transitions 1, 4 and 8, respectively. The spectrum corresponding to the diagonal part of $|\mathrm{GHZ}\rangle\langle\mathrm{GHZ}| - |001\rangle\langle 001|$ state is shown in Figure 11 *d*. It is clearly seen that in the GHZ state (eq. (15)) transitions 1, 3 and 8 have approximately half the intensity of the equilibrium spectrum. Transitions 5, 6 and 7 appear due to POPS. However, to confirm the creation of the GHZ state, a complete tomography of the created GHZ state is needed. The pulse sequence for preparation of POPS, creation of $|\mathrm{GHZ}\rangle\langle\mathrm{GHZ}| - |001\rangle\langle 001|$ state followed by tomography (using experiment (ii) of eq. (13)) is given in Figure 12 *a*. The 2D spectrum corresponding to the measurement of all off-diagonal elements of the GHZ state is shown in Figure 12 *b*. Presence of only triple quantum coherence and absence of all other coherences confirm the creation of the GHZ state. The axial peaks at zero frequency in the vertical dimension are due to the longitudinal relaxation during the t_1 period and imperfections of the 90° pulse (see caption of Figure 4).

Two-qubit DJ using two-dimensional NMR

Implementation of the DJ algorithm on two qubits requires three qubits, including one work qubit. The algorithm can be described as

$$|r\rangle|s\rangle|t\rangle \xrightarrow{U_f} |r\rangle|s\rangle|t \oplus f(r,s)\rangle, \tag{19}$$

$|r\rangle|s\rangle$ and $|t\rangle$ being the states of the two input qubits (I_1, I_2) and the work qubit (I_0), respectively. There are eight possible two-bit binary functions (f), among which two are constant and six are balanced. The transformations corresponding to the constant functions f_1 and f_2 are respectively, unity operator and a π pulse on all the transitions of the work qubit. The unitary transformations encoding the remaining six balanced functions $f_3 - f_8$ are achieved by transition-selective pulses on different transitions (3, 4, 9(*), 6) of the work qubit as [0, 0, π, π], [π, π, 0, 0], [π, 0, π, 0], [0, π, 0, π], [π, 0, 0, π] and [0, π, π, 0] (ref. 38).

The pulse sequence for two-dimensional DJ algorithm is $[(\frac{\pi}{2})^{I_0,I_1,I_2} - t_1 - U_f - \mathrm{Det}(t_2)]$. The transitions of I_1 and I_2 qubits are frequency-labelled during the t_1 period and detected during the t_2 period. Fourier transformation with respect to t_1 and t_2 yields the desired two-dimensional spectrum[39–41]. The experimental result of the above operations on the strongly coupled 3-qubit system of 3-bromo-1,2-dichlorobenzene is given in Figure 13. The experimental results match the expected theoretical results, confirming that two-dimensional DJ algorithm can also be carried out in a strongly coupled three-spin-system.

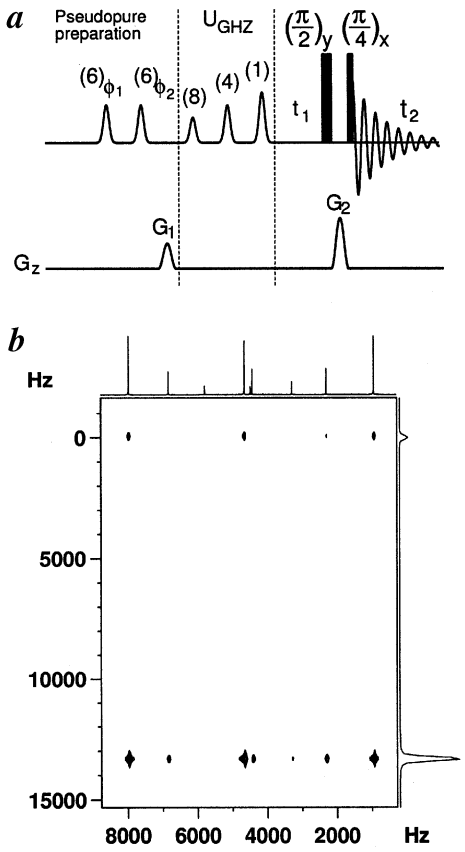

Figure 12. ***a***, Pulse sequence for creation and tomography of $|GHZ\rangle\langle GHZ| - |001\rangle\langle 001|$ state. Numbers inside parentheses indicate transition numbers as shown in Figure 8. G_1 and G_2 are field-gradient pulses of different strengths along the $\hat{z}$-direction. ***b***, Two-dimensional spectrum obtained using the pulse sequence (***a***). Pure triple quantum coherence at $\omega_1 + \omega_4 + \omega_8$ (where ω_k is the frequency of transition k) confirms the creation of the GHZ state.

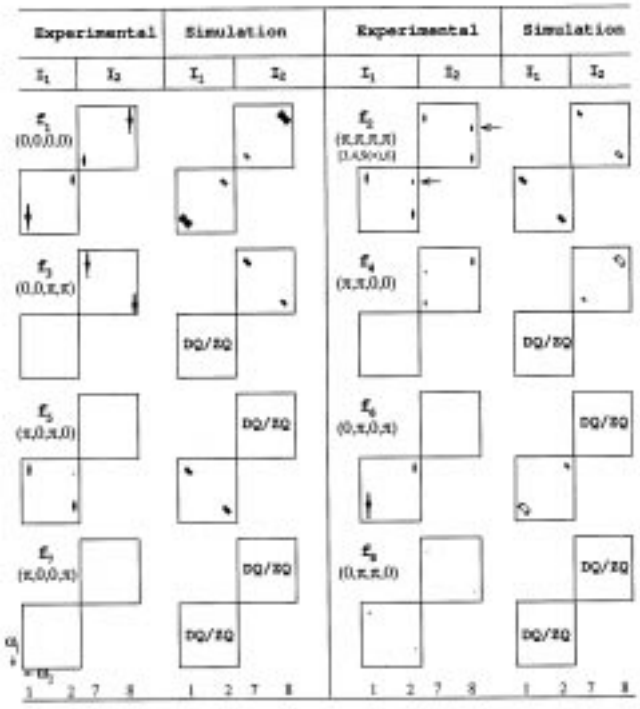

Figure 13. Result of DJ algorithm on 3-bromo-1,2-dichlorobenzene dissolved in ZLI-1132 for various functions $f_1 - f_8$. Only expansions of the transitions of the input qubits (I_1 and I_2) are shown. Expected patterns obtained by GAMMA simulation are also shown against each spectrum. Transitions 3, 4, 9 (*) and 6 are used as the four work-qubit transitions. Interchange of labels 011 ↔ 101 allows us to identify transitions 4 and 9 as those belonging to the 3rd qubit. This does not affect other operations and the four 3rd-qubit transitions, namely 3, 4, 9 and 6 remain unconnected. However, transition 1 now belongs to the 1st qubit (011 ↔ 111) along with transition 2 (010 ↔ 110), and transition 7 to the 2nd qubit (001 ↔ 011) along with transition 8 (000 ↔ 010). All experiments were carried out on a Bruker DRX-500 spectrometer at 300 K. Transition-selective pulses were 1.5, 7.4, 20 and 1.5 ms long, respectively for transitions 3, 4, 9 and 6. Pulse power was then adjusted to make the flip angle of each pulse as π. A phase-cycle of $(x, -x)$ was used to minimize the error of the π pulses during computation. The extra peaks in f_2 (shown by ←) in the experimental spectra originated due to undesired coherence-transfer during computation. All experiments were done using 2048 t_2 and 128 t_1 datapoints. All plots are shown in magnitude mode. Resonance frequencies of various transitions (1, 2, 7 and 8) in ω_2 domain are schematically identified in the bottom line. The π pulses applied to various work-qubit transitions are indicated for each f, with the transitions identified in f_2. The same order follows for other fs. For example, $f_2 = (\pi, \pi, \pi, \pi)$ means π pulses are applied to all the transitions of work qubit and $f_5 = (\pi, 0, \pi, 0)$ means π pulses are applied to transitions 3 and 9, and no pulses to transitions 4 and 6.

Strongly coupled four-spin-system

Labelling of transitions

The system chosen is 2-chloroiodobenzene dissolved in ZLI-1132. The four aromatic protons form a strongly coupled four-spin-system. Equilibrium spectrum is shown in Figure 14. The transitions are labelled according to the descending order of their intensities. The total number of transitions for a four-spin strongly coupled system is ${}^{2\times4}C_{4-1} = 56$, of which only 30 transitions have been observed with sufficient intensity. There are other transitions of smaller intensities comparable to that of ^{13}C satellites. In order to avoid any interference due to ^{13}C satellites, we have used ^{13}C decoupling in the experiment. Decoupling in t_1 dimension is achieved by a single π pulse on ^{13}C channel in the middle of t_1 period, while that in t_2 dimension is carried out by multi-pulse decoupling sequences on the ^{13}C channel. The Z-COSY spectrum obtained after ^{13}C decoupling for the present system is shown in Figure 15. The spectrum consists of more than 2000 peaks. MATLAB analysis of the spectrum has been carried out. Figure 16 *a* shows the connectivity and labelling of the 30 transitions of Figure 14.

Four-qubit gates and pseudopure states

Figure 16 shows implementation of gates and preparation of pairs of pseudopure states using the four-qubit system 2-chloroiodobenzene. The labelling scheme for the energy

levels is shown in Figure 16 *a*. Figure 16 *b* shows the equilibrium spectrum. A C^3-NOT gate can be implemented using a single π pulse on the transition 4. The spectrum corresponding to the C^3-NOT gate obtained using a small-angle detection pulse is shown in Figure 16 *c*. A pair of pseudopure states, namely $|1111\rangle\langle 1111| - |1110\rangle\langle 1110|$ is prepared by subtracting the spectrum in Figure 16 *c* from the equilibrium spectrum shown in Figure 16 *b*. The resultant spectrum is shown in Figure 16 *d*. Similarly, the pair of pseudopure states $|1110\rangle\langle 1110| - |1010\rangle\langle 1010|$ (Figure 16 *e*) is prepared by inverting the transition 1 and subtracting the obtained spectrum from the equilibrium spectrum. Figure 16 *f* demonstrates the implementation of C^2-SWAP gate after preparing the pair of pseudopure states $|1110\rangle\langle 1110| - |1010\rangle\langle 1010|$. The action of C^2-SWAP gate is to interchange the states $|1110\rangle$ and $|1101\rangle$. This is achieved by three transition-selective pulses

$$[\pi^{(4)}.\pi^{(14)}.\pi^{(4)}], \tag{20}$$

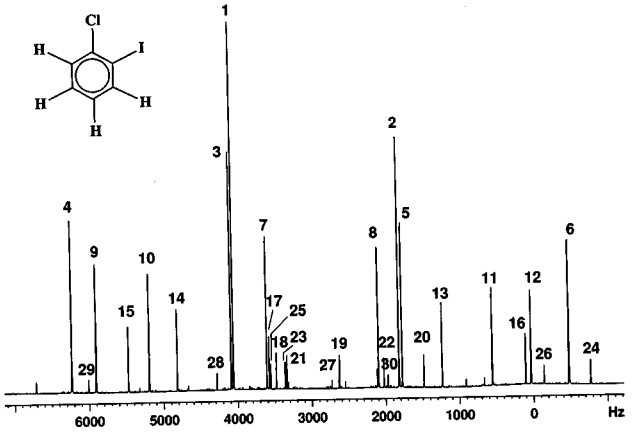

Figure 14. One-dimensional 500 MHz proton spectrum of 2-chloro-iodobenzene oriented in liquid crystal ZLI-1132, at 300 K forming a four-qubit system. Transitions are labelled according to descending order of their intensities.

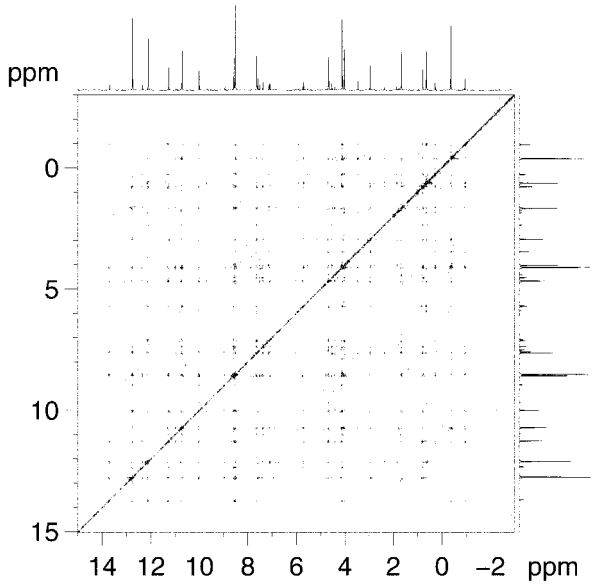

Figure 15. Z-COSY spectrum of the four-spin strongly coupled system shown in Figure 13. The spectrum consists of more than 2000 desired peaks.

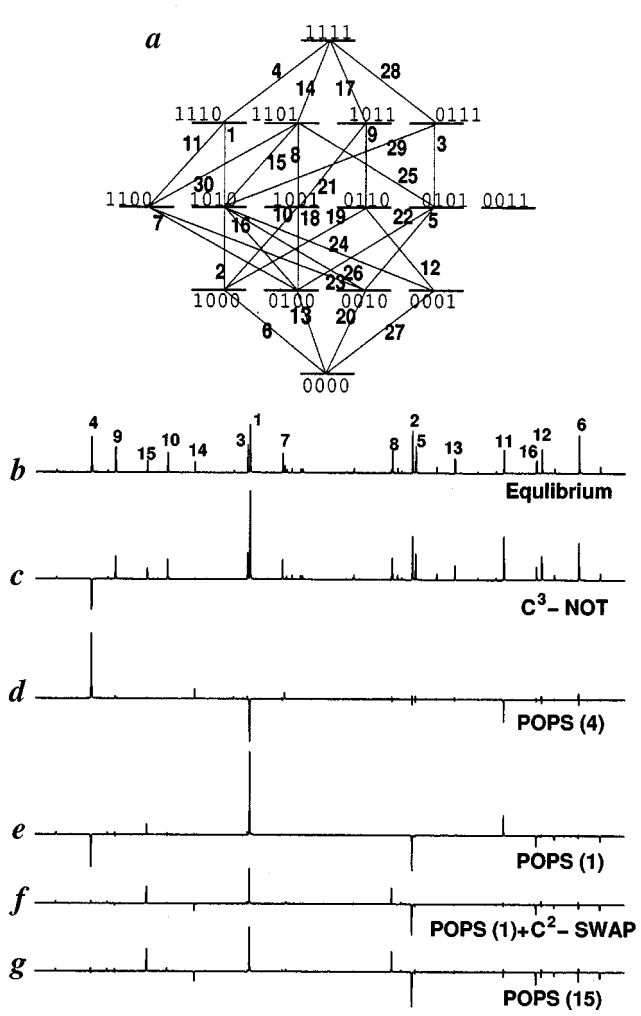

Figure 16. ***a***, Labelling scheme for the states of the four-qubit system of Figure 14. ***b***, Equilibrium spectrum obtained using a small-angle (10°) pulse [the spectra of Figure 14 were obtained using a 90° detection pulse]. ***c***, Spectrum corresponding to C^3-NOT gate obtained by selective inversion of transition number 4 ($|1110\rangle \leftrightarrow |1111\rangle$). ***d***, Spectrum corresponding to the pair of pseudopure states $|1111\rangle\langle 1111| - |1110\rangle\langle 1110|$ obtained by subtracting ***c*** from ***b***, named POPS(4). ***e***, Spectrum corresponding to the pair of pseudopure states $|1110\rangle\langle 1110| - |1010\rangle\langle 1010|$ obtained by inverting the transition 1 and subtracting the obtained spectrum from the equilibrium spectrum ***b***, named POPS(1). ***f***, Spectrum corresponding to the pair of pseudopure states $|1101\rangle\langle 1101| - |1010\rangle\langle 1010|$ obtained by applying C^2-SWAP gate on ***e***. The pulse sequence for C^2-SWAP gate is given in eq. (20). ***g***, Spectrum corresponding to the pair of pseudopure states $|1101\rangle\langle 1101| - |1010\rangle\langle 1010|$ is obtained by inverting the transition 15 and subtracting the spectrum for the equilibrium spectrum ***b***, named POPS(15). Spectra ***f*** and ***g*** match fairly well, indicating good implementation of the C^2-SWAP. All spectra were recorded using a final small-angle (10°) detection pulse to maintain linear response, such that the intensities are proportional to the population differences of the two involved levels only.

where the superscripts indicate the transition numbers. Since the states $|1101\rangle$ and $|1110\rangle$ have almost the same populations in the present case, the spectrum after applying C^2-SWAP gate on equilibrium input state will not be very much different from the equilibrium spectrum. However, if one starts with a pair of pseudopure states $|1110\rangle\langle 1110| - |1010\rangle\langle 1010|$ as the input, the output will be a different pair of pseudopure states,

$$|1110\rangle\langle 1110| - |1010\rangle\langle 1010| \xrightarrow{C^2\text{-SWAP}} |1101\rangle\langle 1101| - |1010\rangle\langle 1010|. \quad (21)$$

The spectrum corresponding to the state $|1101\rangle\langle 1101| - |1010\rangle\langle 1010|$ obtained by applying C^2-SWAP gate on $|1110\rangle\langle 1110| - |1010\rangle\langle 1010|$ is shown in Figure 16 *f*. The pair of pseudopure states $|1101\rangle\langle 1101| - |1010\rangle\langle 1010|$ can also be prepared by inverting the transition 15 and subtracting the spectrum obtained from the equilibrium spectrum, as shown in Figure 16 *g*. The spectra in Figure 16 *f* and *g* match fairly well, indicating good implementation of the C^2-SWAP in Figure 16 *f*.

Conclusion

Increasing the number of qubits in NMR calls for the use of dipolar couplings in oriented homonuclear systems. Such spin systems generally become strongly coupled. Spin selective pulses are not defined in the case of strongly coupled systems. Qubit addressability in such a scenario is achieved through transition-selective pulses. Earlier in weakly-coupled spin-systems, logic gates[20,27,39] and algorithms such as Grover's algorithm and quantum Fourier transform have been implemented[48]. Efforts are going on to implement these algorithms in strongly coupled systems as well as to realize higher qubit systems using nuclear spins oriented in liquid crystal matrices.

1. Shor, P. W., Polynomial-time algorithms for prime factorization and discrete algorithms on quantum computer. *SIAM Rev.*, 1999, **41**, 303–332.
2. Grover, L. K., Quantum mechanics helps in searching for a needle in a haystack. *Phys. Rev. Lett.* 1997, **79**, 325.
3. Preskill, J., Lecture notes for physics 229: quantum information and computation, http://theory.caltech.edu/people/preskill/.
4. Nielsen, M. A. and Chuang, I. L., *Quantum Computation and Quantum Information*, Cambridge University Press, 2000.
5. Bouwmeester, D., Ekert, A. and Zeilinger, A., *The Physics of Quantum Information*, Springer, 2000.
6. Ersnt, R. R., Bodenhausen, G. and Wokaun, A., *Principles of Nuclear Magnetic Resonance in One and Two Dimensions*, Oxford University Press, 1987.
7. Slichter, C. P., *Principles of Magnetic Resonance*, Harper and Row, New York, 1978.
8. Dhiel, P. and Khetrapal, C. L., *NMR-Basic Principles and Progress*, Springer-Verlag, New York, 1996, vol. 1, p. 1995.
9. Yannoni, C. S., Sherwood, M. H., Miller, D. C., Chuang, I. L., Vandersypen, L. M. K. and Kubinec, M. G., Nuclear magnetic resonance quantum computing using liquid crystal solvents. *Appl. Phys. Lett*., 1999, **75**, 3563–3565.
10. Marjanska, M., Chuang, I. L. and Kubinec, M. G., Demonstration of quantum logic gates in liquid crystal nuclear magnetic resonance. *J. Chem. Phys*., 2000, **112**, 5095.
11. Fung, B. M., Using pair of pseudopure states for NMR quantum computing. *Phys. Rev. A*, 2001, **63**, 022304.
12. Mahesh, T. S., Neeraj Sinha, Ramanathan, K. V. and Anil Kumar, Ensemble quantum-information processing by NMR: Implementation of gates and creation of pseudopure states using dipolar coupled spins as qubits. *Phys. Rev. A*, 2002, **66**, 022313.
13. Anil Kumar, Ramanathan, K. V., Mahesh, T. S., Neeraj Sinha and Murali, K. V. R. M., Development in quantum information processing by NMR: Use of quadrupolar and dipolar couplings. *Pramana – J. Phys.*, 2002, **59**, 243–254.
14. Khitrin, A. K. and Fung, B. M., Nuclear magnetic resonance quantum logic gates using quadrupolar nuclei. *J. Chem. Phys.*, 2000, **112**, 6963.
15. Khitrin, A., Sun, H. and Fung, B. M., Method of multifrequency excitation for creating pseudopure states for NMR quantum computing. *Phys. Rev. A*, 2001, **63**, 020301(R).
16. Neeraj Sinha, Mahesh, T. S., Ramanathan, K. V. and Anil Kumar, Toward quantum information processing by nuclear magnetic resonance: Pseudopure states and logical operations using selective pulses on an oriented spin-3/2 nucleus. *J. Chem. Phys.*, 2001, **114**, 4415.
17. Murali, K. V. R. M., Neeraj Sinha, Mahesh, T. S., Malcolm Levitt, Ramanathan, K. V. and Anil Kumar, Quantum information processing by nuclear magnetic resonance: Experimental implementation of half-adder and subtractor operations using an oriented spin-7/2 system. *Phys. Rev. A*, 2002, **66**, 022313.
18. Ranabir Das and Anil Kumar, Use of quadrupolar nuclei for quantum information processing by nuclear magnetic resonance: Implementation of a quantum algorithm. *Phys. Rev. A*, 2003, **68**, 032304.
19. Jones, J. A., NMR quantum computation: A critical evaluation, LANL Archive quant-ph/0002085.
20. Cory, D. G., Dunlop, A. E., Havel, T. F., Somaroo, S. S. and Zhang, W., The effective Hamiltonian of the Pound–Overhauser controlled-NOT gate, LANL Archive: quant-ph/9809045.
21. Benjamin, S. C., Simple pulses for universal quantum computation with a Heisenberg ABAB chain. *Phys. Rev. A*, 2001, **64**, 054303.
22. Cory, D. G., Fahmy, A. F. and Havel, T. F., Ensemble quantum computing by NMR spectroscopy. *Proc. Natl. Acad. Sci. USA*, 1997, **94**, 1634.
23. Gershenfeld, N. and Chuang, I. L., Bulk spin-resonance quantum computation. *Science*, 1997, **275**, 350.
24. Cory, D. G., Price, M. D. and Havel, T. F., Nuclear magnetic resonance spectroscopy: An experimentally accessible paradigm for quantum computing. *Physica D*, 1998, **120**, 82.
25. Knill, E., Chuang, I. L. and Laflamme, R., Effective pure states for bulk quantum computation. *Phys. Rev. A*, 1998, **57**, 3348.
26. Chuang, I. L., Gershenfeld, N., Kubines, M. G. and Leung, D. W., Bulk quantum computation with nuclear magnetic resonance. *Proc. R. Soc. London, Ser. A*, 1998, **454**, 447–467.
27. Kavita Dorai, Arvind and Anil Kumar, Implementing quantum-logic operations, pseudopure states, and the Deutsch–Jozsa algorithm using noncommuting selective pulses in NMR. *Phys. Rev. A*, 2000, **61**, 042306.
28. Mahesh, T. S. and Anil Kumar, Ensemble quantum-information processing by NMR: Spatially averaged logical labelling technique for creating pseudopure states. *Phys. Rev. A*, 2001, **64**, 012307.

29. Knill, E., Laflamme, R., Martinez, R. and Tseng, C. H., An algorithmic benchmark for quantum information processing. *Nature*, 2000, **404**, 368.
30. Peng, X., Zhu, X., Fang, X., Feng, M., Gao, K. and Liu, M., Preparation of pseudopure states by line selective pulses in nuclear magnetic resonanace. *Phys. Rev. A*, 2002, **65**, 042315.
31. Deutsch, D. and Jozsa, R., Rapid solution of problems by quantum computation. *Proc. R. Soc. London, Ser. A*, 1985, **400**, 97.
32. Cleve, R., Ekert, A., Macchiavello, C. and Mosca, M., Quantum algorithms revisited. *Proc. R. Soc. London, Ser. A*, 1998, **454**, 339.
33. Chuang, I. L., Vanderspyen, L. M. K., Zhou, X., Leung, D. W. and Llyod, S., Experimental realization of a quantum algorithm. *Nature*, 1998, **393**, 1443.
34. Jones, J. A. and Mosca, M., Implementation of a quantum algorithm on a nuclear magnetic resonance quantum computer. *J. Chem. Phys*., 1998, **109**, 1648.
35. Lindan, N., Barjat, H. and Freeman, R., An implementation of Deutsch–Jozsa algorithm on a three-qubit NMR quantum computer. *Chem. Phys. Lett*., 1998, **296**, 61.
36. Arvind, Kavita Dorai and Anil Kumar, Quantum entanglement in the NMR implementation of Deutsch–Jozsa algorithm. *Pramana – J. Phys*., 2001, **56**, 705–713.
37. Ranabir Das, Mahesh, T. S. and Anil Kumar, Efficient quantum state tomography for quantum information processing using a two-dimensional Fourier transform technique. *Phys. Rev. A*, 2003, **67**, 062304.
38. Nielsen, M. A. and Chuang, I. L., Programable quantum gate arrays. *Phys. Rev. Lett*., 1997, **79**, 321.
39. Mahesh, T. S. Kavita Dorai, Arvind and Anil Kumar, Implementing logic gates and the Deutsch–Jozsa quantum algorithm by two-dimensional NMR using spin- and transition-selective pulses. *J. Magn. Reson*., 2001, **148**, 95.
40. Madi, Z. L., Bruschweiler, R. and Ernst, R. R., One- and two-dimensional ensemble quantum computing in spin Liouville space. *J. Chem. Phys*., 1998, **109**, 10603.
41. Kavita Dorai, Mahesh, T. S., Arvind and Anil Kumar, Quantum computations by NMR. *Curr. Sci*., 2000, **79**, 1447–1458.
42. Grace, R. C. R. and Anil Kumar, Flip-angle dependence of nono-equilibrium states yielding information on connectivity of transitions and energy levels of oriented molecules. *J. Magn. Reson*., 1992, **99**, 81.
43. Rance, M., Bodenhausen, G., Wagner, G., Wuthrich, K. and Ernst, R. R., A systematic approach to the suppression of *J* cross peaks in 2D exchange and 2D NOE spectroscopy. *J. Magn. Reson.*, 1985, **62**, 497.
44. Greenberger, D. M., Horne, M. and Zeilinger, A., *Bell's Theorem, Quantum Theory and Conceptions of the Universe*, Kluwer, Dordrecht, 1989, pp. 73–76.
45. Greenberger, D. M., Horne, M., Shimony, A. and Zeilinger, A., Bell's theorem without inequalities. *Am. J. Phys*., 1990, **58**, 1131.
46. Laflamme, R., Knill, E., Zurek, W., Catasti, P. and Mariappan, S., NMR GHZ. *Philos. Trans. R. Soc. London, Ser. A*, 1998, **356**, 1941.
47. Richard, J., Nelson, Cory, D. G. and Seth Llyod, Experimental demonstration of Greenberger–Horne–Zeilinger correlations using nuclear magnetic resonanace. *Phys. Rev. A*, 2000, **61**, 022106.
48. Ranabir Das, Mahesh, T. S. and Anil Kumar, Implementation of conditional phase shift gates for quantum information processing by NMR, using transition selective pulses. *J. Magn. Reson*., 2002, **159**, 46.

ACKNOWLEDGEMENTS. We thank Dr Swadhin K. Mandal and Prof. S. S. Krishnamurthy, Department of Inorganic and Physical Chemistry, Indian Institute of Science (IISc), Bangalore for the organometallic compound (I). The use of DRX-500 NMR spectrometer funded by the Department of Science and Technology, New Delhi, at the Sophisticated Instruments Facility, IISc is acknowledged.

Received 24 August 2003